

From Lab to Reality: How Non-AM1.5 Conditions Shape the Future of Perovskite and Organic Solar Cells

Supplementary Information

Zongtai Zhang,^a, Andrew Crossland,^b, Roderick C. I. MacKenzie,^a, Christopher Groves,^{a,*}

I. TEMPERATURE COEFFICIENT AND IRRADIANCE DEPENDENCE

TableS1 presents the temperature coefficient and irradiance dependence of power conversion efficiency (PCE) for the photovoltaics (PV) collected from manufacturers and literature. It includes device type, main materials (technology), PCE under standard test conditions (STC) (PCE_{STC}), normalised PCE at $200W/m^2$ ($nPCE_{200W/m^2}$), temperature coefficient, active areas and source.

N-IBC: Interdigitated Back Contact Technology

PERC: Passivated Emitter Rear Contact solar cell technology

N-TOPCon: Tunnel Oxide Passivated Contact technology

HPDC: High Performance and Hybrid Passivated Dual-Junction Cell

HJT: Heterojunction solar cells

PCE_{STC} : efficiency at Standard test condition

$nPCE_{200W/m^2}$: normalised PCE at $200W/m^2$

TABLE S1: Datasheet of Different PVs

Material	Detail	$PCE_{STC}\%$	$nPCE_{200W/m^2}$	$T_{coe} \%/^\circ C$	Area mm	Source
MonoSi	N-IBC	22.6	/	-0.27	1046*1690	Sunpower[1]
MonoSi	PERC	21.3	/	-0.34	1092*1808	Sunpower[1]
MonoSi	HPDC	23.3	/	-0.28	1134*2382	Longi[2]

^a Department of Engineering, Durham University, South Road, Durham, DH1 3LE, UK.

^b Durham Energy Institute, Durham University, South Road, Durham, DH1 3LE, UK.

*E-mail: chris.groves@durham.ac.uk

MonoSi	HPDC	24.4	/	-0.26	1134*2382	Longi[2]
MonoSi	N-TOPCon	23.4	0.9813	-0.29	1120*2308	JinKo[3]
MonoSi	PERC	22.1	0.9769	-0.35	1134*2278	JinKo[3]
MonoSi	N-TOPCon	23.3	0.9955	-0.29	1134*2382	CanadianSolar[4]
MonoSi	PERC	21.7	/	-0.34	1303*2384	CanadianSolar[4]
MonoSi	HJT	22.3	0.9590	-0.24	1118*1730	REC[5]
MonoSi	PERC	20.8	0.9584	-0.34	1040*1899	REC[5]
MonoSi	N-IBC	22.1	0.9441	-0.29	1039*1895	SPIC Solar[6]
MonoSi	N-TOPCon	22.5	0.9609	-0.3	1134*1762	Qcells[7]
MonoSi	PERC	21.5	0.9604	-0.34	1134*1722	Qcells[7]
MonoSi	N-TOPCon	22.9	0.9860	-0.29	1134*2465	JA Solar[8]
MonoSi	PERC	22.1	0.9878	-0.35	1134*2333	JA Solar[8]
MonoSi	HJT	22.2	/	-0.24	1040*1865	Panasonic[9]
MonoSi	N-TOPCon	22.8	0.9897	-0.29	1134*1762	Trinasolar[10]
MonoSi	PERC	21.8	1.0299	-0.34	1134*1762	Trinasolar[10]
MonoSi	N-TOPCon	22.3	0.9723	-0.29	1042*1740	LG[11]
MonoSi	PERC	21.4	/	-0.38	1029*1864	Silfab Solar[12]
MonoSi	N-TOPCon	23.0	/	-0.30	1303*2384	JOLYWOOD[13]
MonoSi	HJT	22.6	0.9701	-0.26	1302*2383	AE[14]
MonoSi	N-TOPCon	22.6	0.9709	-0.30	1140*1350	AE[14]
MonoSi	PERC	21.3	0.9841	-0.34	1302*2383	AE[14]
MonoSi	HJT	22.0	/	-0.24	1038*1755	belinus[15]
MonoSi	N-IBC	22.3	/	-0.28	1039*1727	belinus[15]
MonoSi	PERC	21.0	/	-0.31	1134*1722	belinus[15]
MonoSi	HJT	23.5	0.9265	-0.24	1303*2384	Phono Solar[16]
MonoSi	N-TOPCon	23.0	0.9695	-0.29	1134*2278	Phono Solar[16]
MonoSi	PERC	21.5	0.9461	-0.33	1134*2278	Phono Solar[16]
MonoSi	HJT	23.1	0.9881	-0.26	1134*2382	HUASUN[17]
MonoSi	N-TOPCon	23.3	0.9884	-0.29	1134*2382	ASTRONERGY[18]
MonoSi	HJT	21.6	/	-0.26	1038*2094	FuturaSun[19]
MonoSi	N-IBC	21.8	/	-0.29	1039*1895	FuturaSun[19]
MonoSi	N-TOPCon	22.8	/	-0.29	1134*2278	FuturaSun[19]
MonoSi	PERC	21.3	/	-0.35	1134*2279	FuturaSun[19]
MonoSi	N-TOPCon	22.7	0.9701	-0.30	1134*2465	YINGLI Solar[20]
MonoSi	PERC	21.5	0.9665	-0.35	1134*2278	YINGLI Solar[20]
MonoSi	HJT	21.7	/	-0.26	1041*1767	MEYER BURGER[21]
MonoSi	HJT	23.3	0.9817	-0.24	1303*2384	risen[22]
MonoSi	N-TOPCon	23.1	0.9802	-0.29	1134*2465	risen[22]

MonoSi	PERC	21.7	0.9838	-0.34	1303*2384	risen[22]
MonoSi	N-TOPCon	23.3	0.9875	-0.29	1134*2278	GCL[23]
MonoSi	PERC	21.9	0.9810	-0.35	1134*2278	GCL[23]
MonoSi	N-TOPCon	22.6	0.9885	-0.29	1134*2278	SUNTECH[24]
MonoSi	PERC	21.5	0.9855	-0.34	1134*2278	SUNTECH[24]
MonoSi	N-TOPCon	22.3	0.9507	-0.32	1133*2278	ADANI[25]
MonoSi	PERC	21.3	0.9444	-0.37	1133*2278	ADANI[25]
MonoSi	HJT	23.2	0.9804	-0.258	1303*2380	SARAPHIM[26]
MonoSi	N-TOPCon	23.0	0.9837	-0.29	1134*2382	SARAPHIM[26]
MonoSi	PERC	21.6	0.9857	-0.34	1303*2384	SARAPHIM[26]
MonoSi	HJT	23.3	0.9804	-0.26	1303*2384	Vikramsol[27]
MonoSi	N-TOPCon	22.5	0.9697	-0.30	1134*2278	Vikramsol[27]
MonoSi	PERC	21.6	0.9685	-0.35	1303*2172	Vikramsol[27]
MonoSi	N-TOPCon	22.5	0.9691	-0.30	1134*2465	ZNSHINE Solar[28]
MonoSi	PERC	21.7	0.9879	-0.35	1134*2279	ZNSHINE Solar[28]
MonoSi	PERC	21.2	/	-0.35	1134*2288	Boviet[29]
MonoSi	N-TOPCon	23.8	0.9014	-0.31	1134*2278	HT-SAAE[30]
MonoSi	HJT	22.9	0.9632	-0.26	1303*2384	HELIENE[31]
MonoSi	N-TOPCon	22.5	0.9627	-0.30	1134*2094	HELIENE[31]
MonoSi	PERC	21.1	0.9657	-0.34	1134*2094	HELIENE[31]
Organic	PM6:AQx-2	15.5	/	-0.107	6 mm ²	Liu et al.[32]
Organic	P3HT:PCBM(MoO ₃)	3.8	/	-0.13	9 mm ²	Lee et al.[33]
Organic	P3HT:PCBM	3.3	/	-0.2	9 mm ²	Lee et al.[33]
Organic	PBDTTT-OFT:PCBM	9.4	/	-0.08	4 mm ²	Xu et al.[34]
Organic	PBDTTT-EFT:PCBM	8.5	/	-0.32	4 mm ²	Xu et al.[34]
Organic	DBP:C ₇₀	6.6	/	-0.113	11.3 mm ²	Burlingame et al.[35]
Organic	PBTZT-stat-BDTT-8	3.3	/	+0.02	1000*6400	Waller et al.[36]
Organic	Heliatek	8	0.9894	0	366*1885	Heliatek[37]
Organic	DIBSQ:PC70BM	4.1	/	+0.4	4mm ²	Chen et al.[38]
Organic	PM6:Y7	15.3	1.0059	/	6mm ²	Wong et al.[39]
Organic	PCDTBT:PC71BM	6.8	0.9551	/	6mm ²	Wong et al.[39]
Organic	PBDB-TF:IT-4F	12.2	1.0340	/	100mm ²	Cui et al.[40]
Organic	PBDB-TF:ITCC	9.8	1.0426	/	100mm ²	Cui et al.[40]
Organic	PBDB-TF:PC71BM	8.4	0.9907	/	100mm ²	Cui et al.[40]
Organic	PCDTBT:PC71BM	6.1	1.2844	/	47.5mm ²	Lechêne et al.[41]
Organic	PBDB-TSCI	13.0	1.0210	/	4.4mm ²	Park et al.[42]
Organic	PBDB-TF	12.1	0.9072	/	4.4mm ²	Park et al.[42]
Organic	PM6:L8-BO	12.5	1.10661	/	4mm ²	Liu et al.[43]

Organic	DTCPB:C70	6.7	1.0022	/	$4mm^2$	Chen et al.[44]
Organic	DTCPO:C70	5.8	1.1266	/	$4mm^2$	Chen et al.[44]
Organic	DTCTB:C70	4.4	1.1386	/	$4mm^2$	Chen et al.[44]
Organic	DTCTBO:C70	3.9	1.1468	/	$4mm^2$	Chen et al.[44]
Perovskite	graphene	12.5	/	-0.21	$910 mm^2$	Pescetelli et al.[45]
Perovskite	Triple Cation	18.5	0.9997	-0.17	$10 mm^2$	Jošt et al.[46]
Perovskite	FAPbI3	10.7	/	-0.12	$9 mm^2$	Zhang et al.[47]
Perovskite	PCBM/FAPbI3	14.6	/	-0.11	$9 mm^2$	Zhang et al.[47]
Perovskite	Triple Cation	5.92	/	+0.0078	$1350 mm^2$	Stoichkov et al.[48]
Perovskite	Triple Cation	20	/	0	$25 mm^2$	Tress et al.[49]
Perovskite	PTAA/MAPbI3	16.4	/	-0.13	$6370 mm^2$	Deng et al.[50]
Perovskite	CsPbI2.85(BrCl)0.15	19.0	/	-0.10	$8.32 mm^2$	Wang et al.[51]
Perovskite	CsPbI2Br	11.3	/	-0.23	$6.25 mm^2$	Dong et al.[52]
Perovskite	PTAA/triple cation	18.1	/	-0.36	$11 mm^2$	Moot et al.[53]
Perovskite	NiOx/triple cation	17.2	/	-0.12	$11 mm^2$	Moot et al.[53]
Perovskite	PTAA/triple halide	15.9	/	-0.25	$11 mm^2$	Moot et al.[53]
Perovskite	NiOx/triple halide	17.9	/	-0.26	$11 mm^2$	Moot et al.[53]
Perovskite	MAPbI3	9.1	/	-0.41	$16 mm^2$	Jacobsson et al.[54]
Perovskite	MAPbI3	12.5	/	-0.23	$20 mm^2$	Leong et al.[55]
Perovskite	MAPbI3	11.3	/	-0.41	$10 mm^2$	Schelhas et al.[56]
Perovskite	MAPbI3	12.3	/	-0.22	$20 mm^2$	Bush et al.[57]
Perovskite	MAPbI3	16.1	/	-0.18	$29.3 mm^2$	Fu et al.[58]
Perovskite	FAPbBr3	10.9	0.9050	-0.3	$14.75 mm^2$	Yue et al.[59]
Perovskite	FA0.9Cs0.1PbI3	16.7	1.1554	/	$9mm^2$	Wong et al.[39]
Perovskite	MAPbI3	12.2	0.8995	/	$40*60$	Ryu et al.[60]
Perovskite	MAPI(500nm)	18.4	1.0447	/	$9mm^2$	Du et al.[61]
Perovskite	MAPI(750nm)	19.0	1.1136	/	$9mm^2$	Du et al.[61]
Perovskite	MAPI(250nm)	18.1	0.9493	/	$9mm^2$	Du et al.[61]
Perovskite	MAPbI3	17.0	0.9397	/	$3.2mm^2$	Troughton et al.[62]
Perovskite	Cs0.15FA0.85PbI3	18.0	0.9586	/	$3.2mm^2$	Troughton et al.[62]
Perovskite	FAMACsPbIBr	20.0	0.9837	/	$9.19mm^2$	Wang et al.[63]
Perovskite	FACsPbIBr	20.7	0.9428	/	$9.19mm^2$	Wang et al.[63]
Perovskite	FAPbI3MAPbBr3	14.4	0.8632	/	$16mm^2$	Reyna et al.[64]

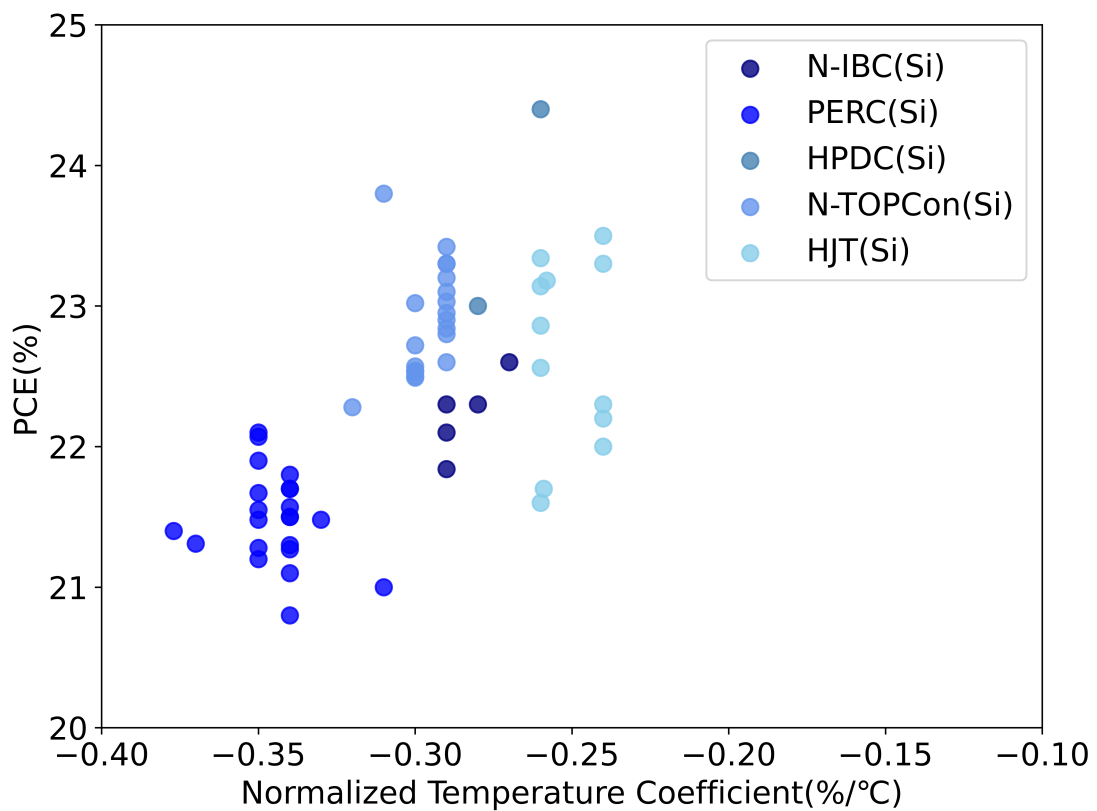


Fig. S1: Temperature coefficient and PCE measured at 25°C for different reported Silicon PV technologies.

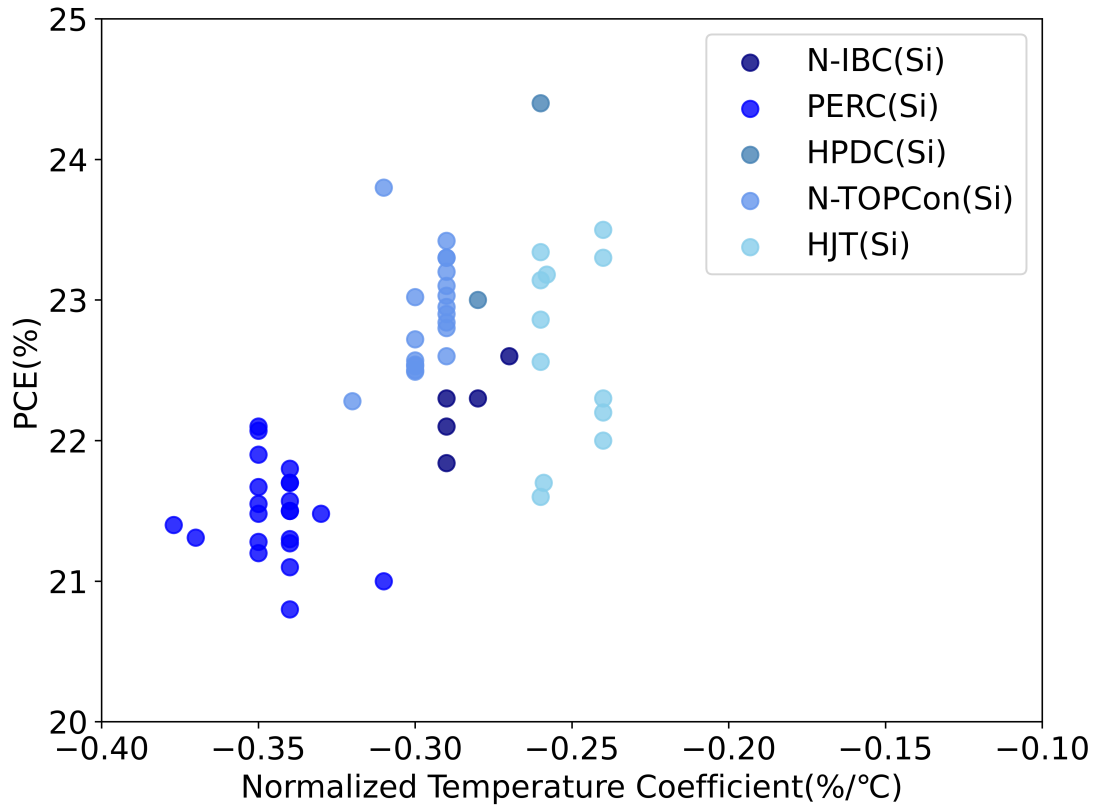


Fig. S2: Difference in PCE measured at 1000 and 200 W/m^2 for different reported Silicon PV technologies.

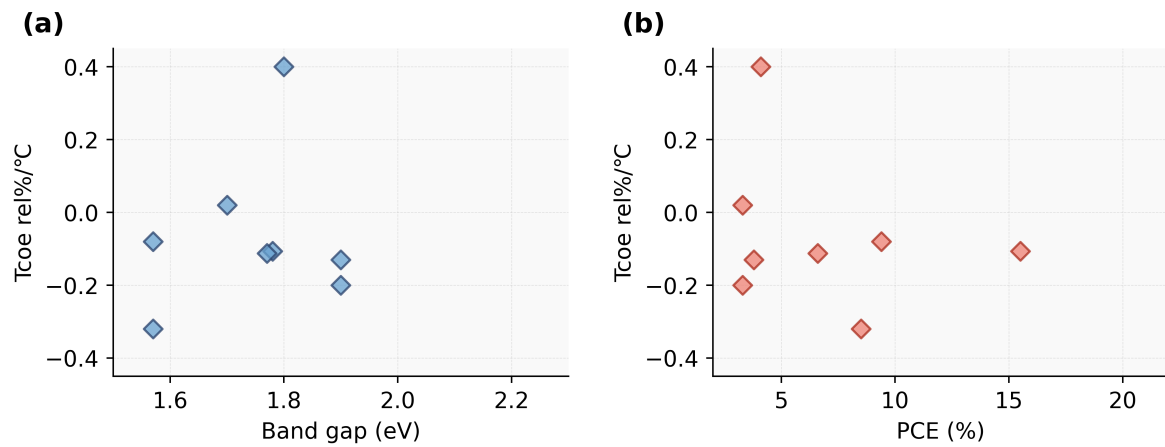


Fig. S3: Temperature coefficient of Organic PV as a function of AM1.5 (a) Band gap and (b) PCE.

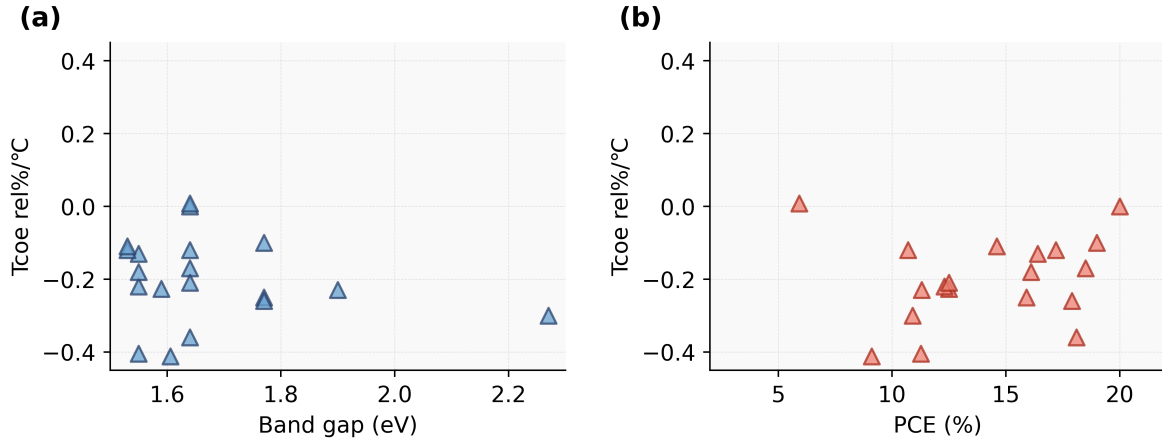


Fig. S4: Temperature coefficient of Perovskite PV as a function of AM1.5 (a) Band gap and (b) PCE.

To examine the possibility that variations in device band-gap might drive differences in observed temperature and irradiance responses, we performed a detailed correlation analysis between band-gap values and these performance metrics across our device dataset. The analysis (Figure S3, S4, S5 and S6) clearly demonstrates that no statistically significant relationship exists between the band-gap and the temperature coefficient or low irradiance performance of the investigated PV devices. This finding indicates that the improved real-world performances reported herein for Perovskite and Organic PV technologies compared to Silicon PV cannot simply be attributed to band-gap variations, but are likely due to intrinsic differences in device architecture and materials.

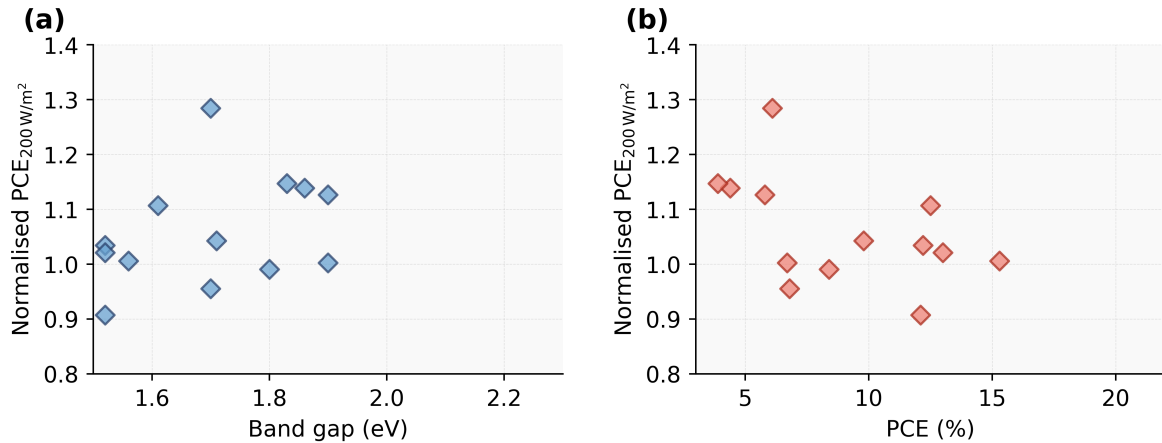


Fig. S5: Normalised PCE at 200 W/m² of Organic PV as a function of AM1.5 (a) Band gap and (b) PCE.

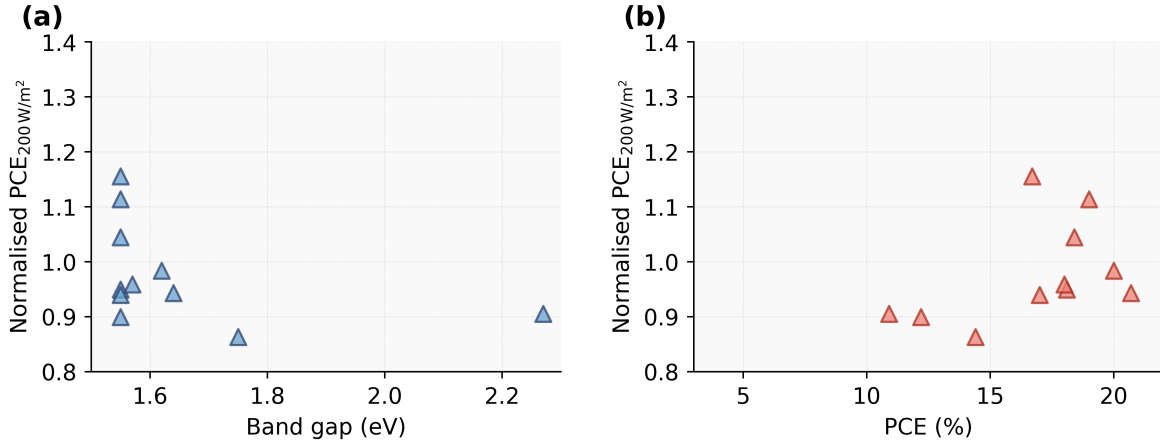


Fig. S6: Normalised PCE at 200 W/m² of Perovskite PV as a function of AM1.5 (a) Band gap and (b) PCE.

II. ROSS COEFFICIENT

The Ross coefficient is used to quantify the effect of wind speed on cell temperature. Figure S7 illustrates the relationship between wind speed and the Ross coefficient for Silicon, Organic, and Perovskite PV technologies.

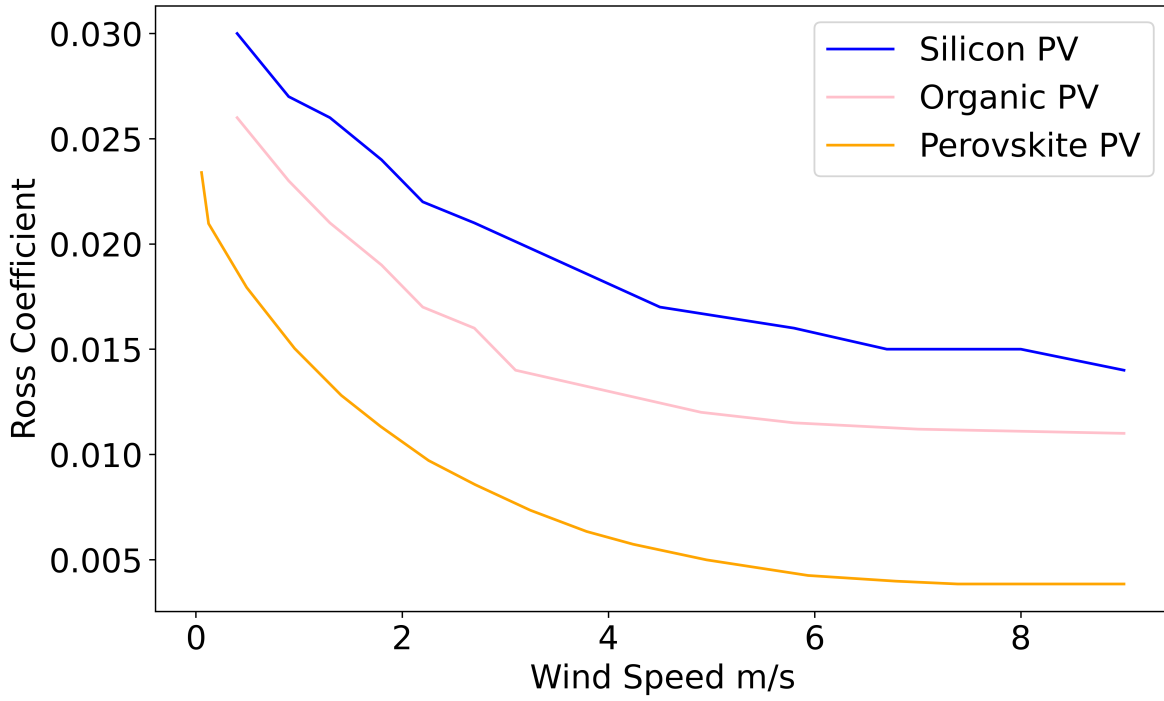


Fig. S7: Effect of wind speed on Ross coefficient.[65]

TABLE S2: Datasheet of selected locations

Location	Latitude	Longitude
London	51.50	0.00
California city	35.00	-118.00
Lisbon	38.75	-9.25

III. SPECIFIC LOCATIONS SELECTED WITHIN ANALYSIS

Within the model, we utilise historical meteorological data (wind speed, irradiance and air temperature) at hourly resolution from the National Solar Radiation Database (NSRDB),[66] along with spectral data computed by the Fast All-Sky Radiation Model for Solar Applications with Narrowband Irradiances on Tilted Surfaces (FARMS-NIT) model for the site of interest. Solar panels are assumed to be ground mounted and have a fixed optimum tilt angle provided by PVGIS.[67] The latitude and longitude of the selected location for weather demonstration and calculation of spectral mismatch factor are provided in Table S2.

IV. GLOBAL VARIATION OF EFFECTIVE EFFICIENCY FOR DIFFERENT PV TECHNOLOGIES

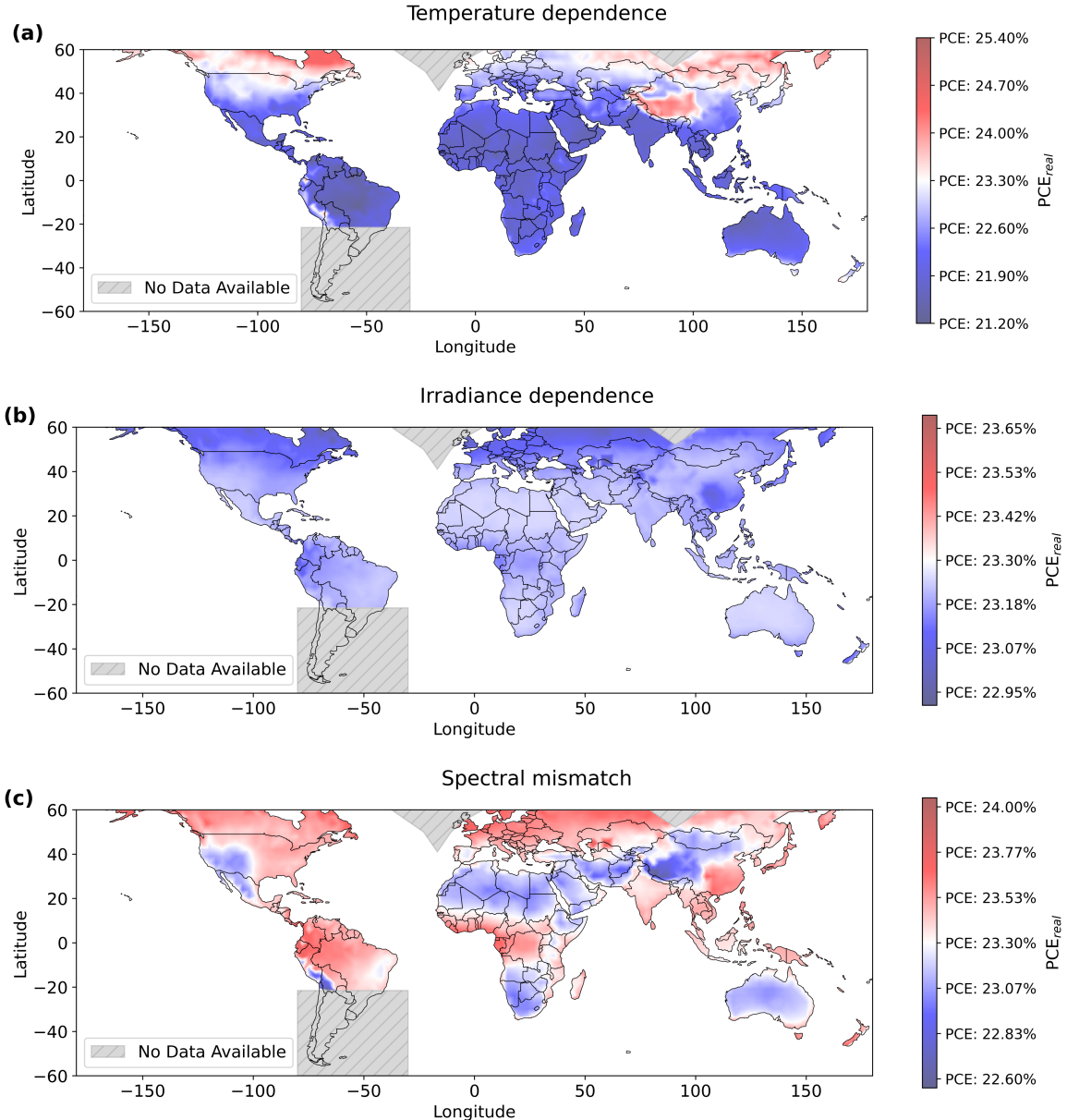


Fig. S8: Predicted PCE_{real} compared to PCE_{STC} for silicon PV across the world in 2019, considering (a) temperature dependence only, (b) irradiance dependence only, and (c) spectral mismatch effect only.

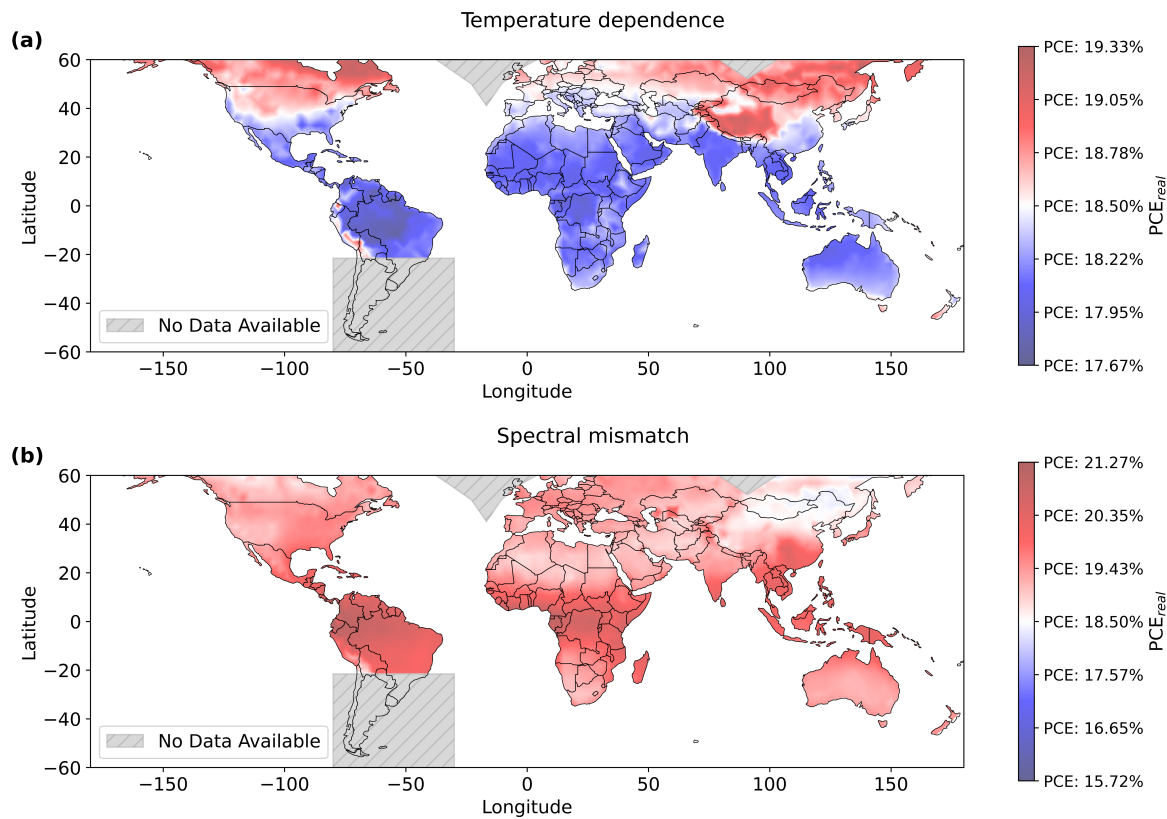


Fig. S9: Predicted PCE_{real} compared to PCE_{STC} for perovskite PV across the world in 2019, considering (a) temperature dependence only and (b) spectral mismatch effect only.

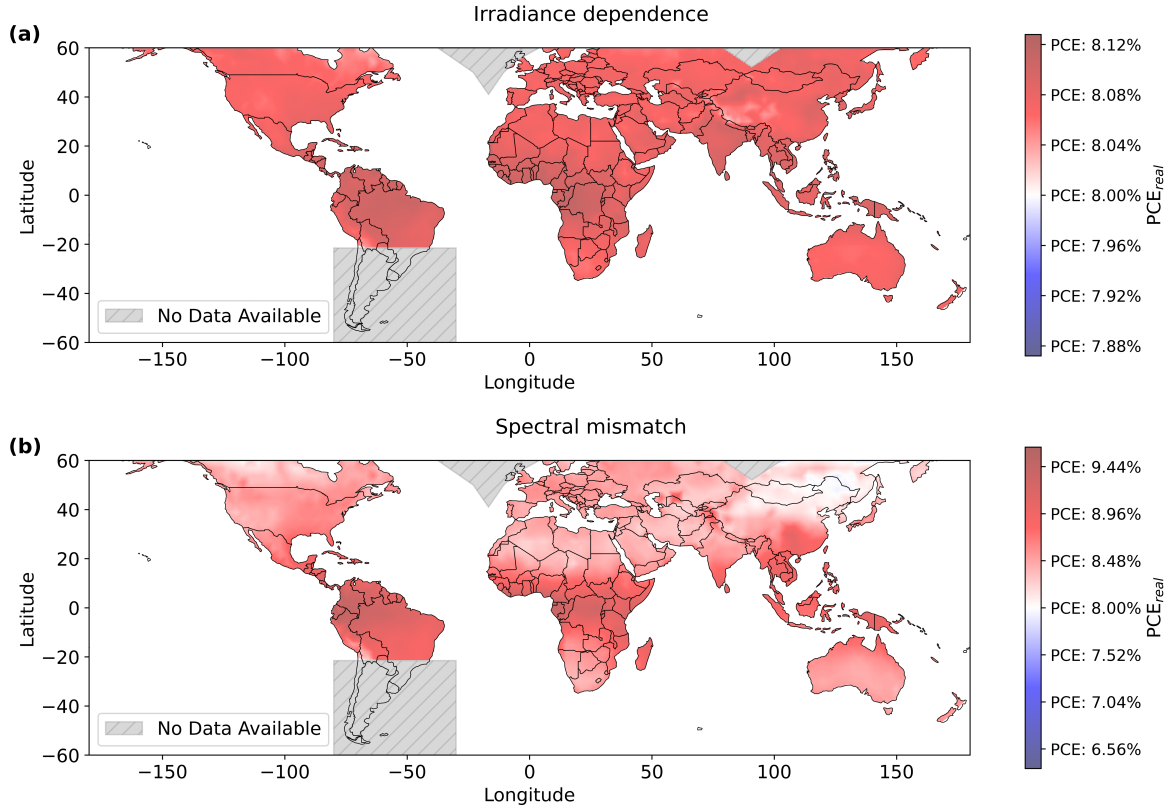


Fig. S10: Predicted PCE_{real} compared to PCE_{STC} for organic PV across the world in 2019, considering (a) irradiance dependence only and (b) spectral mismatch effect only.

This section analyses the impact of temperature, irradiance dependence, and spectral mismatch on Silicon, Perovskite, and Organic PV in global variation scenarios.

Figure S8 illustrates the efficiency variation of Silicon PV. In equatorial regions, Silicon PV suffers up to a 9% loss in efficiency due to high temperatures, reducing its PCE_{real} to 21.20%. Conversely, in colder regions, efficiency increases by up to 5% relative to PCE_{STC} . Across all locations, Silicon PV experiences a decline in efficiency due to irradiance dependence, as the device operates less efficiently in low-light conditions. The efficiency loss due to irradiance ranges from -0.22% to -1.65% of PCE_{STC} . Spectral mismatch effects on silicon PV vary between -3.2% and 2.6%, with losses typically observed at higher altitudes.

For Perovskite PV (Figure S9), irradiance dependence is negligible, so only temperature and spectral mismatch effects are considered. The temperature impact on Perovskite PV follows a similar trend to Silicon but is less severe due to a smaller temperature coefficient, with efficiency changes ranging from -4.3% to 4.5%. Spectral mismatch, however, plays a dominant role, positively affecting Perovskite PV in most regions, with efficiency gains of up to 15%, particularly at higher altitudes.

Finally, for Organic PV (Figure S10), temperature has no effect due to its zero temperature coefficient. The

device benefits slightly from irradiance, with a 0.3% to 1% efficiency improvement. However, spectral mismatch has a significant impact, ranging from -2% to 20.5%. The distribution of spectral mismatch effects for Organic PV closely resembles that of Perovskite PV, as both technologies exhibit strong absorption in the short-wavelength region.

REFERENCES

- [1] Maxeon Solar Technologies, “Maxeon solar panels,” 2024, accessed: 2024-07-08. [Online]. Available: <https://sunpower.maxeon.com/int/solar-panel-products/maxeon-solar-panels>
- [2] LONGi Solar, “Downloads - solar panels,” 2024, accessed: 2024-07-08. [Online]. Available: <https://www.longi.com/en/download/?categoryId=28&productClassificationId=271>
- [3] Jinko Solar, “Jinko solar products,” 2024, accessed: 2024-07-08. [Online]. Available: <https://www.jinkosolar.com/en/site/dwparametern>
- [4] CSI Solar, “Downloads,” 2024, accessed: 2024-07-08. [Online]. Available: <https://www.csisolar.com/downloads?downid=19483>
- [5] REC Group, “Rec group solar panels,” 2024, accessed: 2024-07-08. [Online]. Available: <https://www.recgroup.com/en>
- [6] SPIC Solar, “Spic solar products,” 2024, accessed: 2024-07-08. [Online]. Available: <http://en.spicsolar.com/default/servers/11.html>
- [7] Q CELLS, “Solar panels for private customers,” 2024, accessed: 2024-07-08. [Online]. Available: <https://www.q-cells.co.uk/private-customers/solar-panels>
- [8] JA Solar, “Ja solar products,” 2024, accessed: 2024-07-08. [Online]. Available: <https://www.jasolar.com/index.php?m=content&c=index&a=lists&catid=453>
- [9] Panasonic, “Panasonic solar support,” 2024, accessed: 2024-07-08. [Online]. Available: <https://na.panasonic.com/us/solarsupport?series=78566&product=93511>
- [10] Trina Solar, “Resources and downloads - trina solar,” 2024, accessed: 2024-07-08. [Online]. Available: <https://www.trinasolar.com/eu-en/resources/downloads#TSM-DEG5-2>
- [11] LG Solar, “Lg-neon-r-lg405q1c-a6,” 2024, accessed: 2024-07-08. [Online]. Available: <https://www.lg.com/us/business/neon-r/lg-lg405q1c-a6>
- [12] Silfab Solar, “Silfab-elite-sil-410-bg,” 2024, accessed: 2024-07-08. [Online]. Available: <https://silfabsolar.com/our-solar-panels/silfab-elite/sil-410-bg/>
- [13] Jolywood, “Niwa pro product details,” 2024, accessed: 2024-07-08. [Online]. Available: <http://www.jolywood.cn/en/product?id=12&area=NIWA%20Pro>
- [14] AE Solar, “Catalogue,” 2024, accessed: 2024-07-08. [Online]. Available: <https://ae-solar.com/catalogue>

- [15] Belinus, “Solar panels,” 2024, accessed: 2024-07-08. [Online]. Available: <https://belinus.com/en/solar-panels>
- [16] Phono Solar, “Solar modules,” 2024, accessed: 2024-07-08. [Online]. Available: <http://www.phonosolar.com/?SolarModules/>
- [17] Huasun Solar, “G12r new products,” 2024, accessed: 2024-07-08. [Online]. Available: <https://www.huasunsolar.com/g12r-new-products/>
- [18] Astronergy, “Download center,” 2024, accessed: 2024-07-08. [Online]. Available: https://www.astronergy.com/download-center/?down_type=4#down
- [19] FuturaSun, “Downloads,” 2024, accessed: 2024-07-08. [Online]. Available: <https://www.futurasun.com/en/download/#17001436726255a18a9d3abe8>
- [20] Yingli Solar, “Downloads,” 2024, accessed: 2024-07-08. [Online]. Available: https://www.yinglisolar.com/en/download_127.html
- [21] Meyer Burger, “Downloads,” 2024, accessed: 2024-07-08. [Online]. Available: <https://www.meyerburger.com/en/downloads#c23394>
- [22] Risen Energy, “Downloads,” 2024, accessed: 2024-07-08. [Online]. Available: https://en.risenenergy.com/serve/download?two_level2
- [23] GCL-SI, “Solar modules,” 2024, accessed: 2024-07-08. [Online]. Available: https://en.gclsi.com/modules?product_catalog15
- [24] Suntech Power, “Ultra v series,” 2024, accessed: 2024-07-08. [Online]. Available: <https://www.suntech-power.com/products/ultravseries/>
- [25] Adani Solar, “Downloads,” 2024, accessed: 2024-07-08. [Online]. Available: <https://www.adanisolar.com/Downloads>
- [26] Seraphim Energy, “Downloads,” 2024, accessed: 2024-07-08. [Online]. Available: <https://www.seraphim-energy.com/services/downloads/>
- [27] Vikram Solar, “Pv modules,” 2024, accessed: 2024-07-08. [Online]. Available: <https://www.vikramsol.com/pv-modules/>
- [28] ZNSHine Solar, “Downloads,” 2024, accessed: 2024-07-08. [Online]. Available: <https://www.znshinesolar.com/downloadshome.html>
- [29] Boviet Solar, “Perc cell technology,” 2024, accessed: 2024-07-08. [Online]. Available: <https://bovietsolar.com/technology/perccelltechnology>
- [30] HT-SAAE, “Products,” 2024, accessed: 2024-07-08. [Online]. Available: <https://www.ht-saae.com.au/products/>
- [31] Heliene, “Products,” 2024, accessed: 2024-07-08. [Online]. Available: <https://heliene.com/products/>
- [32] W. Liu, S. Sun, and X. Zhu, “Organic photovoltaics integrated with thermoelectric generator achieving low

- critical temperature difference and efficient energy conversion,” *Advanced Functional Materials*, vol. 32, no. 13, p. 2109410, 2022.
- [33] D. Lee, J. Kim, G. Park, H. W. Bae, M. An, and J. Y. Kim, “Enhanced operating temperature stability of organic solar cells with metal oxide hole extraction layer,” *Polymers*, vol. 12, no. 4, p. 992, 2020.
- [34] X. Xu, K. Fukuda, A. Karki, S. Park, H. Kimura, H. Jinno, N. Watanabe, S. Yamamoto, S. Shimomura, D. Kitazawa *et al.*, “Thermally stable, highly efficient, ultraflexible organic photovoltaics,” *Proceedings of the National Academy of Sciences*, vol. 115, no. 18, pp. 4589–4594, 2018.
- [35] Q. Burlingame, G. Zanotti, L. Ciammaruchi, E. A. Katz, and S. R. Forrest, “Outdoor operation of small-molecule organic photovoltaics,” *Organic Electronics*, vol. 41, pp. 274–279, 2017.
- [36] R. Waller, M. Kacira, E. Magadley, M. Teitel, and I. Yehia, “Evaluating the performance of flexible, semi-transparent large-area organic photovoltaic arrays deployed on a greenhouse,” *AgriEngineering*, vol. 4, no. 4, pp. 969–992, 2022.
- [37] Heliatek, “Datasheet HeliaSol 436-2000,” <https://www.heliatek.com>, 2023, accessed: 24 March 2024.
- [38] G. Chen, C. Si, Z. Tang, K. Guo, T. Wang, J. Zhang, and B. Wei, “Temperature-dependent device performance of organic photovoltaic cells based on a squaraine dye,” *Synthetic Metals*, vol. 222, pp. 293–298, 2016.
- [39] V. K. Wong, C. Zhang, Z. Zhang, M. Hao, Y. Zhou, and S. K. So, “0.01 to 0.5 sun is a realistic and alternative irradiance window to analyze urban outdoor photovoltaic cells,” *Materials Today Energy*, p. 101347, 2023.
- [40] Y. Cui, H. Yao, T. Zhang, L. Hong, B. Gao, K. Xian, J. Qin, and J. Hou, “1 cm² organic photovoltaic cells for indoor application with over 20% efficiency,” *Advanced Materials*, vol. 31, no. 42, p. 1904512, 2019.
- [41] B. P. Lechêne, M. Cowell, A. Pierre, J. W. Evans, P. K. Wright, and A. C. Arias, “Organic solar cells and fully printed super-capacitors optimized for indoor light energy harvesting,” *Nano Energy*, vol. 26, pp. 631–640, 2016.
- [42] S. Park, H. Ahn, J.-y. Kim, J. B. Park, J. Kim, S. H. Im, and H. J. Son, “High-performance and stable nonfullerene acceptor-based organic solar cells for indoor to outdoor light,” *ACS Energy Letters*, vol. 5, no. 1, pp. 170–179, 2019.
- [43] X. Liu, X. Liu, Z. Xia, Y. Ji, D. Zhang, Y. Cheng, X. Liu, J. Yuan, X. Yang, and W. Huang, “A semitransparent organic solar cell with a bifacial factor of 99.1%,” *Materials Today Energy*, p. 101614, 2024.
- [44] C.-H. Chen, H.-C. Ting, Y.-Z. Li, Y.-C. Lo, P.-H. Sher, J.-K. Wang, T.-L. Chiu, C.-F. Lin, I.-S. Hsu, J.-H. Lee *et al.*, “New d-a-a-configured small-molecule donors for high-efficiency vacuum-processed organic photovoltaics under ambient light,” *ACS applied materials & interfaces*, vol. 11, no. 8, pp. 8337–8349, 2019.
- [45] S. Pescetelli, A. Agresti, G. Viskadouros, S. Razza, K. Rogdakis, I. Kalogerakis, E. Spiliarotis, E. Leonardi, P. Mariani, L. Sorbello *et al.*, “Integration of two-dimensional materials-based perovskite solar panels into a

- stand-alone solar farm,” *Nature Energy*, vol. 7, no. 7, pp. 597–607, 2022.
- [46] M. Jošt, B. Lipovšek, B. Glažar, A. Al-Ashouri, K. Brecl, G. Matič, A. Magomedov, V. Getautis, M. Topič, and S. Albrecht, “Perovskite solar cells go outdoors: field testing and temperature effects on energy yield,” *Advanced energy materials*, vol. 10, no. 25, p. 2000454, 2020.
- [47] X. Zhang, Y. Guan, Y. Zhang, W. Yu, C. Wu, J. Han, Y. Zhang, C. Chen, S. Zheng, and L. Xiao, “Achieving small temperature coefficients in carbon-based perovskite solar cells by enhancing electron extraction,” *Advanced Optical Materials*, vol. 10, no. 23, p. 2201598, 2022.
- [48] V. Stoichkov, N. Bristow, J. Troughton, F. De Rossi, T. Watson, and J. Kettle, “Outdoor performance monitoring of perovskite solar cell mini-modules: diurnal performance, observance of reversible degradation and variation with climatic performance,” *Solar Energy*, vol. 170, pp. 549–556, 2018.
- [49] W. Tress, K. Domanski, B. Carlsen, A. Agarwalla, E. A. Alharbi, M. Graetzel, and A. Hagfeldt, “Performance of perovskite solar cells under simulated temperature-illumination real-world operating conditions,” *Nature energy*, vol. 4, no. 7, pp. 568–574, 2019.
- [50] Y. Deng, C. H. Van Bracke, X. Dai, J. Zhao, B. Chen, and J. Huang, “Tailoring solvent coordination for high-speed, room-temperature blading of perovskite photovoltaic films,” *Science advances*, vol. 5, no. 12, p. eaax7537, 2019.
- [51] F. Wang, Z. Qiu, Y. Chen, Y. Zhang, Z. Huang, N. Li, X. Niu, H. Zai, Z. Guo, H. Liu *et al.*, “Temperature-insensitive efficient inorganic perovskite photovoltaics by bulk heterojunctions,” *Advanced Materials*, vol. 34, no. 9, p. 2108357, 2022.
- [52] Z. Dong, W. Li, H. Wang, X. Jiang, H. Liu, L. Zhu, and H. Chen, “High-temperature perovskite solar cells,” *Solar RRL*, vol. 5, no. 9, p. 2100370, 2021.
- [53] T. Moot, J. B. Patel, G. McAndrews, E. J. Wolf, D. Morales, I. E. Gould, B. A. Rosales, C. C. Boyd, L. M. Wheeler, P. A. Parilla *et al.*, “Temperature coefficients of perovskite photovoltaics for energy yield calculations,” *ACS Energy Letters*, vol. 6, no. 5, pp. 2038–2047, 2021.
- [54] T. J. Jacobsson, W. Tress, J.-P. Correa-Baena, T. Edvinsson, and A. Hagfeldt, “Room temperature as a goldilocks environment for $\text{CH}_3\text{NH}_3\text{PbI}_3$ perovskite solar cells: the importance of temperature on device performance,” *The Journal of Physical Chemistry C*, vol. 120, no. 21, pp. 11 382–11 393, 2016.
- [55] W. L. Leong, Z.-E. Ooi, D. Sabba, C. Yi, S. M. Zakeeruddin, M. Graetzel, J. M. Gordon, E. A. Katz, and N. Mathews, “Identifying fundamental limitations in halide perovskite solar cells,” *Advanced Materials*, vol. 28, no. 12, pp. 2439–2445, 2016.
- [56] L. T. Schelhas, J. A. Christians, J. J. Berry, M. F. Toney, C. J. Tassone, J. M. Luther, and K. H. Stone, “Monitoring a silent phase transition in $\text{CH}_3\text{NH}_3\text{PbI}_3$ solar cells via operando x-ray diffraction,” *ACS Energy*

- Letters*, vol. 1, no. 5, pp. 1007–1012, 2016.
- [57] K. A. Bush, C. D. Bailie, Y. Chen, A. R. Bowring, W. Wang, W. Ma, T. Leijtens, F. Moghadam, and M. D. McGehee, “Thermal and environmental stability of semi-transparent perovskite solar cells for tandems enabled by a solution-processed nanoparticle buffer layer and sputtered ito electrode,” *Advanced Materials*, vol. 28, no. 20, pp. 3937–3943, 2016.
- [58] F. Fu, T. Feurer, T. P. Weiss, S. Pisoni, E. Avancini, C. Andres, S. Buecheler, and A. N. Tiwari, “High-efficiency inverted semi-transparent planar perovskite solar cells in substrate configuration,” *Nature Energy*, vol. 2, no. 1, pp. 1–9, 2016.
- [59] W. Yue, H. Yang, H. Cai, Y. Xiong, T. Zhou, Y. Liu, J. Zhao, F. Huang, Y.-B. Cheng, and J. Zhong, “Printable high-efficiency and stable fapbbr3 perovskite solar cells for multifunctional building-integrated photovoltaics,” *Advanced Materials*, vol. 35, no. 36, p. 2301548, 2023.
- [60] S. Ryu, D. C. Nguyen, N. Y. Ha, H. J. Park, Y. H. Ahn, J.-Y. Park, and S. Lee, “Light intensity-dependent variation in defect contributions to charge transport and recombination in a planar mapbi3 perovskite solar cell,” *Scientific reports*, vol. 9, no. 1, p. 19846, 2019.
- [61] T. Du, W. Xu, S. Xu, S. R. Ratnasingham, C.-T. Lin, J. Kim, J. Briscoe, M. A. McLachlan, and J. R. Durrant, “Light-intensity and thickness dependent efficiency of planar perovskite solar cells: charge recombination versus extraction,” *Journal of Materials Chemistry C*, vol. 8, no. 36, pp. 12 648–12 655, 2020.
- [62] J. Troughton, N. Gasparini, and D. Baran, “Cs 0.15 fa 0.85 pbi 3 perovskite solar cells for concentrator photovoltaic applications,” *Journal of Materials Chemistry A*, vol. 6, no. 44, pp. 21 913–21 917, 2018.
- [63] Z. Wang, Q. Lin, B. Wenger, M. G. Christoforo, Y.-H. Lin, M. T. Klug, M. B. Johnston, L. M. Herz, and H. J. Snaith, “High irradiance performance of metal halide perovskites for concentrator photovoltaics,” *Nature Energy*, vol. 3, no. 10, pp. 855–861, 2018.
- [64] Y. Reyna, M. Salado, S. Kazim, A. Pérez-Tomas, S. Ahmad, and M. Lira-Cantu, “Performance and stability of mixed fapbi3 (0.85) mapbbr3 (0.15) halide perovskite solar cells under outdoor conditions and the effect of low light irradiation,” *Nano Energy*, vol. 30, pp. 570–579, 2016.
- [65] N. Bristow and J. Kettle, “Outdoor organic photovoltaic module characteristics: Benchmarking against other pv technologies for performance, calculation of ross coefficient and outdoor stability monitoring,” *Solar Energy Materials and Solar Cells*, vol. 175, pp. 52–59, 2018.
- [66] M. Sengupta, Y. Xie, A. Lopez, A. Habte, G. MacLaurin, and J. Shelby, “The national solar radiation data base (nsrdb),” *Renewable and sustainable energy reviews*, vol. 89, pp. 51–60, 2018.
- [67] T. Huld, R. Müller, and A. Gambardella, “A new solar radiation database for estimating pv performance in europe and africa,” *Solar Energy*, vol. 86, no. 6, pp. 1803–1815, 2012.